Hindawi
Advances in Materials Science and Engineering
Volume 2017, Article ID 8410895, 9 pages
https://doi.org/10.1155/2017/8410895

Research Article

Experimental Study on Ultrahigh Strength Concrete Filled Steel Tube Short Columns under Axial Load

Xiaojun Zhou,[1] Tingmin Mou,[2] Hongyuan Tang,[1] and Bikun Fan[2]

[1]*School of Architecture and Civil Engineering, Xihua University, Chengdu 610039, China*
[2]*Sichuan Provincial Transport Department Highway Planning, Survey, Design and Research Institute, Chengdu 610041, China*

Correspondence should be addressed to Hongyuan Tang; tanghyseu@163.com

Received 8 February 2017; Revised 22 June 2017; Accepted 6 July 2017; Published 6 August 2017

Academic Editor: Bernd-Arno Behrens

Copyright © 2017 Xiaojun Zhou et al. This is an open access article distributed under the Creative Commons Attribution License, which permits unrestricted use, distribution, and reproduction in any medium, provided the original work is properly cited.

Based on the project of Modaoxi Bridge, an experimental study on the compressive behavior of ultrahigh strength concrete filled steel tube (UHSCFST) short column was conducted. A total of 9 UHSCFST specimens were tested, and the cube strength (f_{cu}) of the core concrete reached 115.4 MPa. Main parameters were the confining factor (ξ = 0.608, 0.919, and 1.015), steel ratio (α = 14.67%, 20.02%, and 21.98%), and steel strength (f_y = 349 MPa, 352 MPa, and 427 MPa). The axially loading test results showed that the visible damage of steel tube occurred under the ultimate load. The higher the confining effect, the less the damage features. And all specimens basically presented a drum-type failure mode. The confining effect of steel tube effectively changed the brittle failure mode of ultrahigh strength concrete (UHSC) and tremendously improved the load bearing capacity and ductility of specimens. Moreover, the higher the steel ratio and steel strength of the specimens, the stronger the confining effect. Meanwhile the excellent mechanical properties will be obtained. Also it is recommended that the UHSCFST prefers Q345 or above strength steel tube to ensure sufficient ductility, and the steel ratio should be more than 20%. Furthermore, the confining effect of steel tubes can improve the ultimate bearing capacity of the ultrahigh strength CFST short columns.

1. Introduction

Concrete filled steel tube (CFST) is a kind of composite structure material, which consists of thin-walled steel tubes and concrete. CFST has been widely used in the civil engineering due to its high capacity, good plasticity, excellent seismic resistance, and convenient construction properties. There are also some other kinds of composite materials, such as the double-skin FRP-HSC-steel columns (DSTCs) [1–3] and concrete filled FRP tubes (CFFTs) [4]. However, many steel tubes in current projects were mainly filled with the ordinary concrete [5–7], but with the development of ultrahigh strength concrete (UHSC), the ultrahigh strength concrete filled steel tube (UHSCFST) with core concrete strength exceeding C80 has been gradually applied in the civil engineering. For example, in Japan, UHSCFST columns with 160 MPa UHSC were used in Techno Station, and UHSCFST with 150 MPa UHSC was used in Abeno Harukas [8]. Moreover, in China, with the highway gradually extending to the mountains from the plain, a large number of high-pier and long-span bridges need to be built and all of them need the UHSC. Therefore, the number of the UHSCFST in bridge engineering is gradually increasing, as shown in Table 1. In particular, the UHSCFST is suitable for mountain bridges, which can not only improve bearing capacity and construction efficiency of this kind of bridge, but also reduce the amount of materials and bridge weight.

It has been found that the higher the strength of concrete, the greater the brittleness. The tests by Tan and Pu [9] show that compared with the ordinary CFST, the strength and plastic deformation of UHSC will be significantly improved due to the confinement effect of steel tube, the same as the bearing capacity of UHSCFST. The authors [10–13] also reached similar conclusions. However, Liew and Xiong [14, 15] described that the UHSCFST has strong bearing capacity, but the load versus axial displacement curves tended to drop quickly after peak loads. The UHSCFST presented brittle fracture characteristics, and the confinement effect of steel tube was not obvious before the peak load. Therefore, the confinement effect should not be taken into account when calculating the ultimate bearing capacity of the specimens. Meanwhile, further experimental investigations were carried

Table 1: UHSCFST bridge in China.

Country	Grade of concrete	Application project	Year of application
China	C80	Labajin Bridge in Yaxi Expressway, Sichuan Province. Pier height: 182.5 meters	2008
China	C80	Zhaohua Jialingjiang Bridge, Guangyuan, Sichuan Province. Span: 364 meters	2011
China	C100	Modaoxi Bridge in Xugu Expressway, Sichuan Province. Span: 280 meters	2015
China	C100	Guanshen Qujiang Bridge, Guang'an, Sichuan Province. Span: 320 meters	Under construction

(a) Assemble of rigid skeleton (b) Construction of reinforced concrete arch (c) View of Modaoxi Bridge

Figure 1: Modaoxi Bridge, steel tube in rigid skeleton filled with C100 UHSC.

out by Tao et al. [16], Tokgoz and Dundar [17], and Lu et al. [18] aiming at improving the ductile behavior of the UHSCFST. And it was found that adding steel fibres in core concrete is the most effective method. However, test results reported in [19] show that the strengthening effect of reinforcing bars in core concrete is better than that of adding the steel fibre. Furthermore, Zhang and Wang [20, 21] analyzed the deformation characteristics and failure mechanism of high strength concrete filled steel tube under axial compression and concluded that the high strength concrete should be matched with the high strength steel. Xiong and Liew [22] conducted an experimental study on the fire resistance of high strength concrete filled steel tube columns. Generally speaking, the experimental study on axial compressive behavior of UHSCFST short columns with C80 strength concrete or above is still on the way, and the current design guides are only applicable for the normal strength concrete. For example, Eurocode 4 limits the concrete strength grade only up to C60, and the limitation of Chinese specifications is C80. Additional work should be done to reveal the mechanical properties of UHSCFST to promote its application in practice.

For this case, based on the project of Modaoxi Bridge, an experimental investigation of UHSCFST short columns with core concrete compression strength up to C100 is presented in this study. The main objective is to analyze the properties of UHSCFST short columns, such as the local and global failure process, deformation performance, and ultimate bearing capacity. Then check the applicability of Chinese specifications. This paper will be helpful for the application of UHSCFST and provide experimental support for the revision of the relevant regulations and codes.

2. Project Profile

Modaoxi Bridge is located in Gulin County in Sichuan Province in China, and it is a reinforced concrete arch bridge with a span of 280 meters. And the UHSCFST rigid skeleton was used in the construction of reinforced concrete main arch, as shown in Figure 1. However, the rigid skeleton bears the load together with the main arch during the bridge operation stage. The steel tube in rigid skeleton filled with UHSC of strength grade up to C100 and a self-compacting concrete of C50 was used in reinforced concrete arch.

3. Experimental Programs

3.1. Material Properties

3.1.1. Concrete. The raw materials of concrete came from the Modaoxi Bridge, and the mix proportion and key properties are listed in Table 2. Figure 2 shows the concrete mixture, which has good cohesiveness, encapsulation, and fluidity. And the slump and slump flow were 235 mm and 600 mm, respectively. The concrete cube strength (f_{cu})

Table 2: Concrete mix proportion and key properties.

Mix proportion/kg/m^3									Working ability/mm		f_{cu}/MPa	
Cement	Silica fume	Fly ash	Mineral powder	Expansion agent	Sand	Gravel	Water	Water reducer	Slump	Slump flow	7 d	28 d
480	60	50	35	50	609	1235	126	13.8	235	600	98.7	115.4

Figure 2: Status of the concrete mixture.

Figure 3: Failure mode of C100 UHSC.

reached 115.4 MPa after 28 days. After failure, the specimens were broken into pieces as shown in Figure 3, which presented the obvious brittle characteristics. And the stress-strain curves described in Figure 4 are almost straight lines. Therefore, effective measures should be taken to improve the brittleness of UHSC so as to ensure its safe application in civil engineering.

3.1.2. Steel Tube. The steel tube specimens were cut to the desired lengths. Care was taken to ensure square and flat ends.

Three kinds of circular steel tubes with different section sizes were used, and steel types included Q235 and Q345 (nominal yield strength of 235 MPa and 345 MPa, respectively). The actual mechanical properties of the steel tubes were obtained by coupon test, as shown in Table 3.

3.2. Test Specimens. There were 9 UHSCFST specimens tested under axial load. These tests were designed to investigate the effects of three major parameters on their axial compression behaviors: the steel ratio (α), the yield strength of steel tube (f_y), and the confining factor (ξ). The specimens were further classified into three groups, S1, S2, and S3,

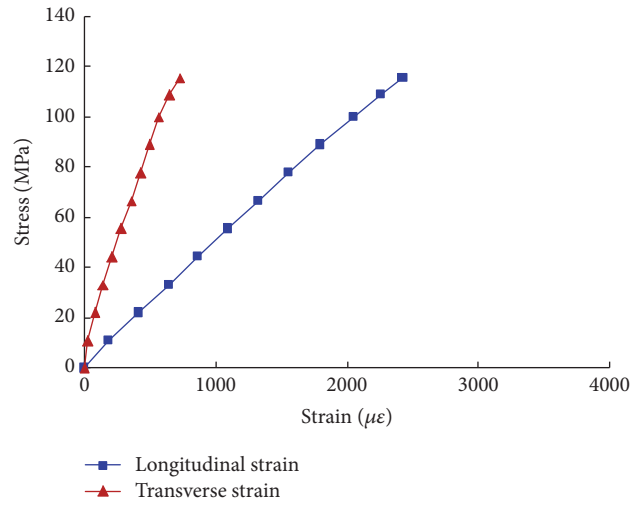

Figure 4: Stress-strain curves.

corresponding to their different steel ratios of 14.67%, 20.02%, and 21.98%, respectively. And each group contained 3 identical specimens to check the reliability of the experimental program. The details of all specimens are summarized in Table 4, in which the two terms of label S*x*-*x* represent the group and number, respectively. And the test confining factor ξ_t ($\xi_t = A_s f_y / A_c f_c$) and displacement ductility factor μ ($\mu = \Delta y^{0.85} / \Delta y$) are also listed in Table 4, where A_s and f_y are the cross-section area and yield strength of steel tube, respectively; A_c and f_c ($f_c = 0.73 f_{cu}$) are section area and prism compressive strength of core concrete; $\Delta y^{0.85}$ is the axial shortening at 85% of the ultimate load in the descending branch of axial load-axial shortening curve, and Δy is the axial shortening at the yield load (D is defined as diameter, t is defined as thickness, and L is defined as length).

3.3. Test Procedure

3.3.1. Test Setup and Instrumentation. The tests were conducted using a universal testing machine with a capacity of 10000 kN in the laboratory of Sichuan Provincial Transport Department Highway Planning, Survey, Design and Research Institute. The test setup, locations of strain gauges, and LVDTs are shown in Figure 5. The specimen was placed on the loading plate of the testing machine, which was connected with the machine through the ball hinge. For each specimen, eight strain gauges mounted on the specimen surface were installed to measure the longitudinal and transverse strains at the mid-height of the steel tube. Two linear variable differential transducers (LVDTs) were located symmetrically to record the axial shortenings.

Table 3: Mechanical properties of the steel tubes.

Dimensions $D \times t \times L$/mm	Types	Yield strength/MPa	Tensile strength/MPa	Elasticity modulus ($\times 10^5$)/MPa
$127 \times 4.2 \times 480$	Q235	349	487	2.01
$133 \times 5.8 \times 480$	Q345	427	573	2.11
$203 \times 9.6 \times 800$	Q235	352	516	2.09

Table 4: Specimen properties and test results.

Group	Specimen	$D \times t \times L$/mm	α/%	f_c/MPa	f_y/MPa	ξ_t	$N_u{}^t$/kN	Δy/mm	$\Delta y^{0.85}$/mm	μ
S1	S1-1	$127 \times 4.2 \times 480$	14.67%	84.2	349	0.608	2205	2.04	6.01	2.94
	S1-2	$127 \times 4.2 \times 480$	14.67%	84.2	349	0.608	2245	2.00	6.30	3.15
	S1-3	$127 \times 4.2 \times 480$	14.67%	84.2	349	0.608	2254	1.94	5.85	3.02
S2	S2-1	$133 \times 5.8 \times 480$	20.02%	84.2	427	1.015	3112			
	S2-2	$133 \times 5.8 \times 480$	20.02%	84.2	427	1.015	3187		/	
	S2-3	$133 \times 5.8 \times 480$	20.02%	84.2	427	1.015	3193			
S3	S3-1	$203 \times 9.6 \times 800$	21.98%	84.2	352	0.919	5988			
	S3-2	$203 \times 9.6 \times 800$	21.98%	84.2	352	0.919	5906		/	
	S3-3	$203 \times 9.6 \times 800$	21.98%	84.2	352	0.919	6010			

3.3.2. Loading Procedure. Three times preloading was carried out prior to the testing, at a rate of 600 N/sec for group 1 and group 2 and 800 N/sec for group 3, respectively. The preload was no more than 30% of its estimated yield load (estimated by (3)).

The loading procedure was in three steps: (1) Prior to yielding of the steel tube, a load interval of less than one-tenth of the estimated yield load was used at a rate of 1000 N/sec for group 1 and group 2 and 1500 N/sec for group 3, respectively. And for each load interval maintained for 2 min, then the strain and axial shortening were recorded. (2) Hereafter, the axial load was applied continuously with a loading speed of 1.0 mm/min for group 1 and group 2 and 1.5 mm/min for group 3, respectively. (3) When the load increased to 80% of the ultimate load or a visible deformation was observed, a displacement control mode was performed until the axial load came back to zero.

4. Experimental Results and Discussions

4.1. Test Observations and Failure Modes. Except specimen S2-3, no cracks occurred in steel tubes during axial loading. The axial load and shortening deformation were linearly increased in the early stages of loading, and there was no visible damage on the outer surface of the steel tubes. A transverse expansion of UHSC occurred until the compressive stress closed to its ultimate bearing capacity; then, a visible damage occurred on external surface of UHSCFST. When the load increased to about 95% of the ultimate bearing capacity, it could be observed that the rust stains fell off, and slip lines appeared on steel tubes of group S1 specimens. The slip lines were the outline of the drum-type failure on the surface of the steel tube. Meanwhile, a sound of concrete cracking could also be heard. However, for the group S2 and group S3 specimens, no other phenomenon occurred but the rust stains fell off. After the peak load, it could be seen that local buckling occurred at the upper and lower end of the specimens; meanwhile the load capacity gradually decreased. Subsequently, the local buckling could also be found in the middle of the specimens when the load dropped to about 85% of the ultimate load. And the axial shortening deformation of the specimens accelerated while the decrease of the load slowed down inversely. Finally, the UHSCFST specimens presented a drum-type failure, as shown in Figure 6. The confining effect of group S2 and group S3 specimens was more than that of group S1 specimens and the same as the confinement effect of steel tubes on the core concrete. Therefore, compared with the group S1 specimens, the group S2 and group S3 specimens presented inconspicuous failure characteristics.

4.2. Axial Load versus Axial Shortening Deformation Curves. Figure 7 shows the axial load versus axial shortening curves of the tested specimens, where the axial shortening is the average value of two LVDTs. As it can be seen, the curves of all the three group specimens have both ascending and descending parts. The curves behaved approximately in a linear phase prior to the yielding of the tested specimens, and the linear phases were longer than that of the ordinary CFST. A similar phenomenon was also reported in previous literature [9]. The main reason was attributed to the fact that the stress-strain curve of UHSC was almost a straight line before the ultimate strength, as shown in Figure 4. And then, the axial load versus axial shortening curves of UHSCFST specimens entered the elastic-plastic stage until the load increased to about 85% of the ultimate bearing capacity. After that, a peak load appeared at the curves, which corresponded to the ultimate bearing capacity of the specimens. Finally, the bearing capacity decreased gradually. The smaller the confining effect was, the more significant the bearing capacity decreased. However, it could also be seen that the three group specimens presented excellent postpeak

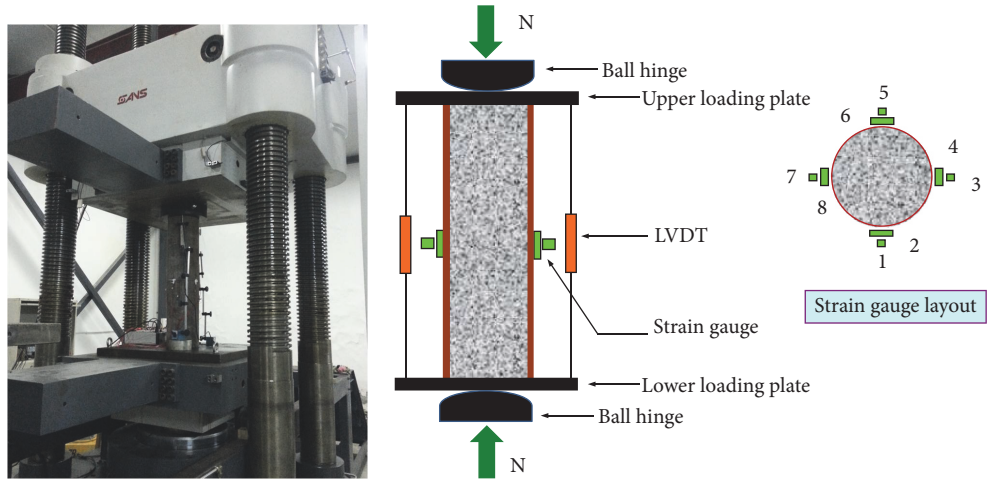

Figure 5: Test setup (a) and locations of strain gauges and LVDTs (b).

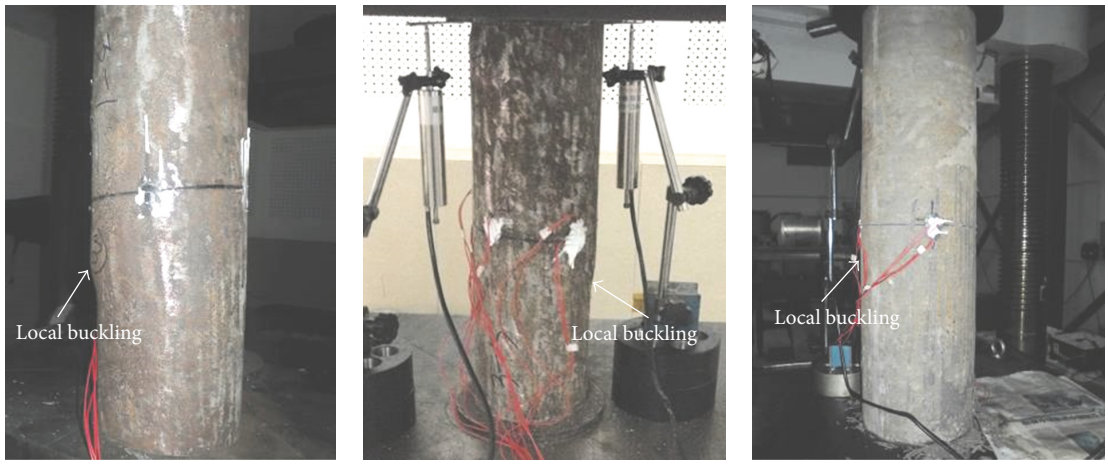

Figure 6: Typical failure modes of the UHSCFST specimens.

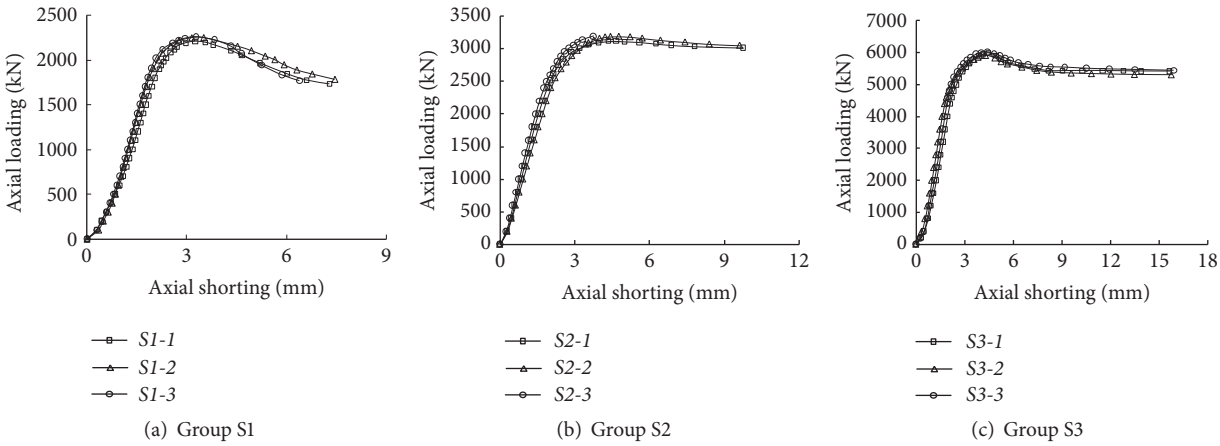

Figure 7: Axial load versus axial shortening curves.

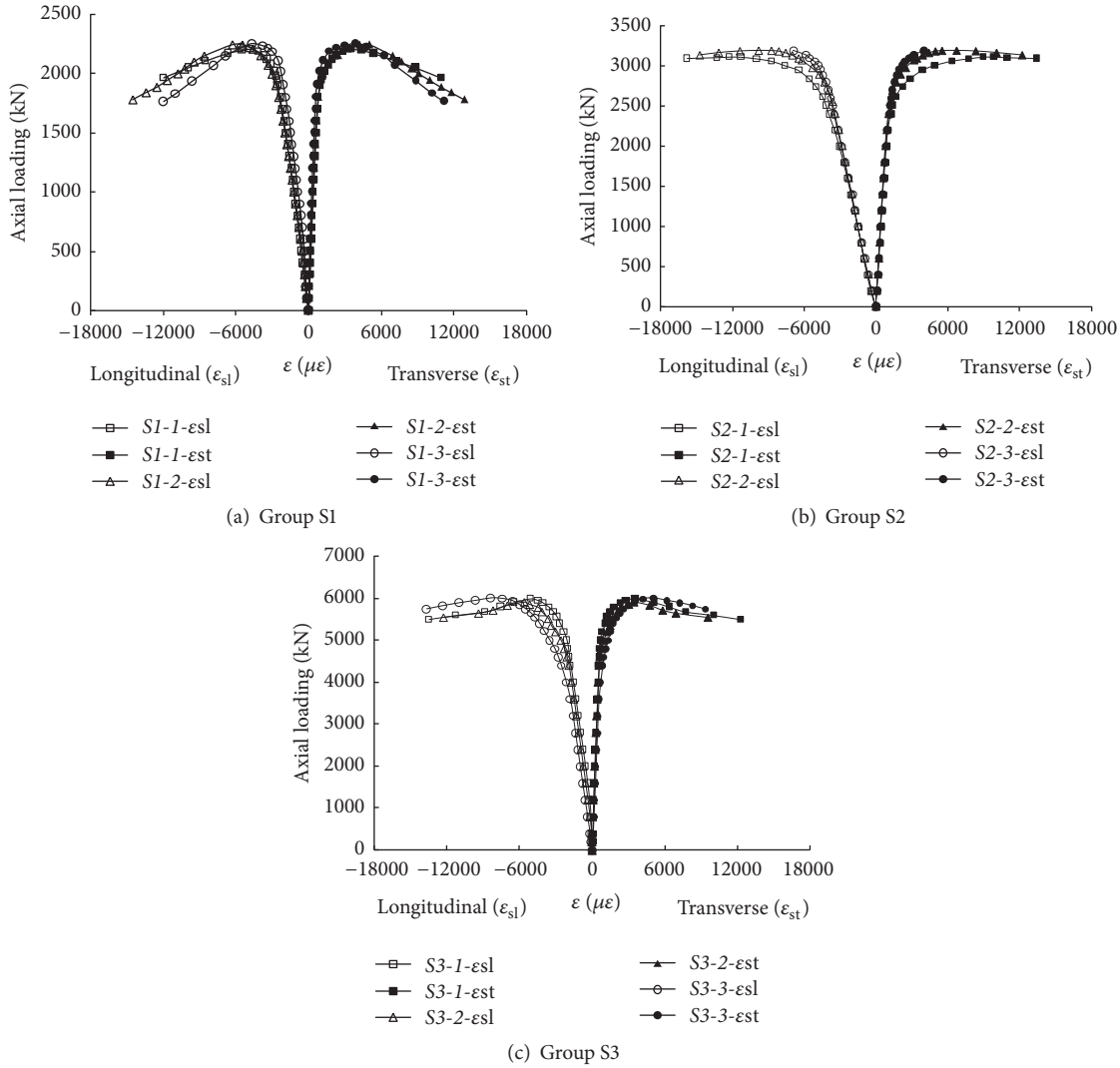

Figure 8: Axial load versus strain curves.

behaviors: even the axial shortening rate of the group S2 and S3 specimens reached 2%, and the residual bearing capacity of the specimens still exceeded 85% of the ultimate bearing capacity; for the group S1 specimens, when the bearing capacity decreased to 85% of the ultimate bearing capacity, the ductility coefficient was up to 3.04. This demonstrated the fact that the confining effect of steel tube on UHSC was obvious due to the confining effect of steel tube; meanwhile, the development of UHSC cracks was effectively restricted, thus making the HUSCFST short columns have prominent ductility performance.

It can also be found from Figure 7 that there are some differences in the postpeak behaviors of three group specimens. Compared with the group S1 and group S2 specimens, the outer diameters of steel tubes were similar, but the group S2 specimens had higher steel ratio and steel strength, so that more significant confining factor and stronger confining effect were obtained in the group S2 specimens. As thus, the slope of the postpeak descending branch is more moderate for the group S2 specimens, which dictates a better ductile behavior. For group S3 specimens, the steel ratios were more than that of group S2, but the steel strength was lower. Hence, relatively smaller confining factor and weaker confining effect were obtained compared with group S2 specimens. Therefore, the bearing capacity decreased obviously. Thus it may be concluded that, in order to obtain ultrahigh bearing capacity and ductility, UHSCFST short columns should have high steel ratio, and also the high strength steel tube should be preferred.

However, because the ultimate load of all the specimens was obtained from the loading test, the slip lines of the curves in Figure 7 were not complete. And that does not affect the results.

4.3. Axial Load versus Strain Curves. Typical relationships between the measured axial load and the steel strain (ε) of the tested specimens are compared in Figure 8, where the longitudinal (ε_{sl}) and transverse (ε_{st}) steel strains are the average of 4 strain gauges and denoted as positive and negative, respectively. Figure 9 shows relationships of typical

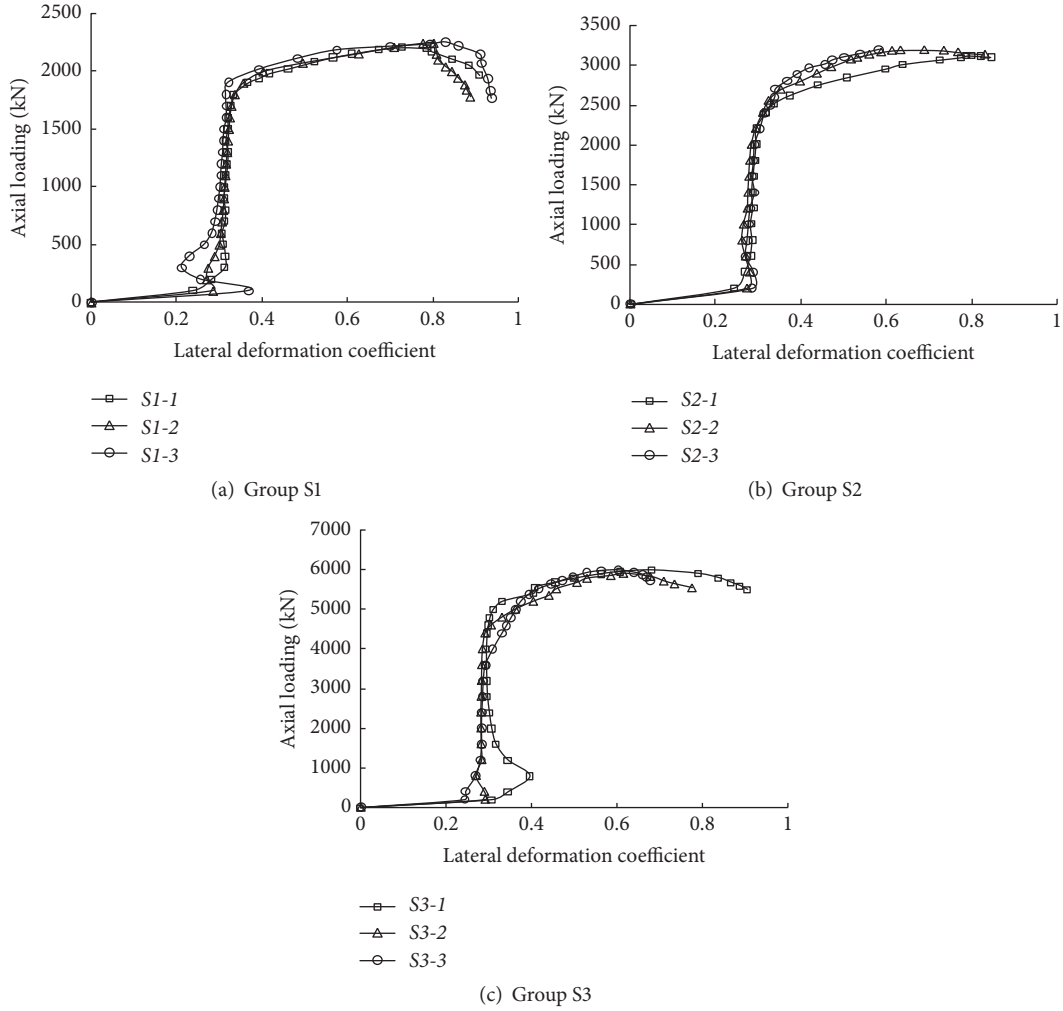

Figure 9: Axial load versus lateral deformation coefficient curves.

axial load versus lateral deformation coefficient (absolute value of ratio of longitudinal to transverse strain, $|\varepsilon_{st}/\varepsilon_{sl}|$). It could be seen that the longitudinal and transverse strains increased linearly at the initial loading stage, and the lateral deformation coefficients were close to Poisson's ratio of steel ($\mu_s = 0.273$). Then lateral deformation coefficients increased significantly when the load increased to about 85% of the ultimate bearing capacity. It indicated that core concrete lateral expansion occurred due to the initiation of microcracks. So the radial pressure of the steel tube obviously improved and led to the fact that the growth rate of the transverse strains was faster than that of the longitudinal strains. It was also observed that, compared to the other two groups, lateral deformation coefficients of the group S2 specimens changed more moderately. Once again, this attributes to the fact that the group S2 specimens have higher confining factor and stronger confinement effect of steel tubes on the core concrete. Meanwhile, after the peak load, the strains of the group S2 specimens increased continuously, but the bearing capacity did not decrease, which presented excellent mechanical properties such as steel. This revealed the fact that the brittle failure behavior of UHSC would be changed by the confining effect of steel tube, and the UHSCFST has ultrahigh bearing capacity and excellent plastic deformation ability.

4.4. Improvement of Bearing Capacity. According to the superposition principle, the nominal bearing capacity ($N_u{}^n$) of UHSCFST short columns can be obtained by adding the ultimate bearing capacity of the steel tube and the core concrete (1), in which the confining effect of the steel tube is ignored. The nominal bearing capacities of the tested specimens are listed in Table 5, and the ratios of the measured bearing capacity to the nominal bearing capacity are also listed in this table.

$$N_u{}^n = A_s f_y + A_c f_c. \tag{1}$$

It can be observed that the measured ultimate bearing capacities ($N_u{}^t$) of the tested specimens were higher than the nominal bearing capacities ($N_u{}^n$). This demonstrated the fact that the confining effect of steel tube played an important role in improving the axial load bearing capacity of the specimens. The steel tubes in the group S3 and group S1 specimens were Q235, and the strength of them were almost

Table 5: Comparisons between calculated ultimate strengths and test results.

Group	Specimen	D/t	α/%	f_y/MPa	ξ_t	N_u^t/kN	Nominal capacity		Unified strength theory		Limit analysis theory	
							N_u^n/kN	N_u^t/N_u^n	N_u^u/kN	N_u^t/N_u^u	N_u^l/kN	N_u^t/N_u^l
S1	S1-1	30.2	14.67%	349	0.608	2205	1496	1.474	1878	1.174	2062	1.069
	S1-2	30.2	14.67%	349	0.608	2245	1496	1.501	1878	1.195	2062	1.089
	S1-3	30.2	14.67%	349	0.608	2254	1496	1.507	1878	1.200	2062	1.093
S2	S2-1	22.9	20.02%	427	1.015	3112	1965	1.584	2546	1.222	2955	1.053
	S2-2	22.9	20.02%	427	1.015	3187	1965	1.622	2546	1.252	2955	1.079
	S2-3	22.9	20.02%	427	1.015	3193	1965	1.625	2546	1.254	2955	1.081
S3	S3-1	20.9	21.98%	352	0.919	5988	4288	1.396	5663	1.057	6342	0.944
	S3-2	20.9	21.98%	352	0.919	5906	4288	1.377	5663	1.043	6342	0.931
	S3-3	20.9	21.98%	352	0.919	6010	4288	1.402	5663	1.061	6342	0.948

the same. The steel ratios of group S3 specimens were higher, so the confining effects were larger. The ratio of measured ultimate bearing capacities to the calculated bearing capacity N_u^t/N_u^n was smaller than that of group S1 specimens. For the group S2 specimens, the Q345 steel tubes were used, and the steel strength and steel ratio were higher than those of group S1. Thus, the confining effect was also larger than that of group S1. However, compared to group S3 specimens, the ratio of the measured ultimate bearing capacities to the calculated bearing capacities N_u^t/N_u^n was larger than that of group S1. This phenomenon might indicate that, in order to effectively exert the confining effect of steel tube on UHSC, the higher strength concrete filled steel short column needs higher steel ratio and higher strength steel. Similar results were also reported in previous literature [4]. Therefore, it could be inferred that the excellent mechanical properties of UHSCFST were not only affected by the comprehensive parameters of the confining effect, but also with the reasonable matching of steel ratio and steel strength. Based on the results of this experiment, it is suggested that the C100 or above grade concrete should be combined with Q345 or above strength grade steel tube to form UHSCFST, and the steel ratio should be no less than 20%.

4.5. Calculation Method of Axial Bearing Capacity. The confining effect of steel tube to core concrete had obvious effect on the bearing capacity of UHSCFST short columns; therefore, the influence of confining effect should be taken into account when calculating the axial bearing capacity. At present, the axial compression bearing capacity calculation methods of normal CFST which considered the confining effect include two types: unified strength theory and limit analysis theory calculation method. For example, the Chinese specifications were CECS28: 2012 and JTDG/T D65-60; see (2) and (3) respectively. The two calculation methods were used to calculate the compression bearing capacity of the tested specimens and then compared with the test results. The results are shown in Table 5, where N_u^u and N_u^l are the calculated results of CECS28: 2012 and JTDG/T D65-60, respectively. The main purpose was to investigate whether the methods were applicable to the axial bearing capacity calculation of UHSCFST.

The limit analysis theory calculation method [23] is

$$\theta \le 1.235\text{: } N_u = A_c f_c (1 + 2\theta),\ \theta = \frac{A_s f_y}{A_c f_c},$$
$$\theta > 1.235\text{: } N_u = A_c f_c \left(1 + \sqrt{\theta} + 1.1\theta\right). \tag{2}$$

And the unified strength theory calculation method [24] is

$$N_u = (1.14 + 1.02\xi)\, f_c \times A_{sc}. \tag{3}$$

The comparison results in Table 5 show that the tested ultimate bearing capacity N_u^t of group S1, group S2, and group S3 specimens was 19.0%, 24.27%, and 5.37% higher than the results (N_u^u) of the unified strength theory and 8.37%, 7.10%, and −5.90% more or less than the results (N_u^l) of the limit analysis theory. The main reason was attributed to the fact that the bearing capacity of UHSCFST was mainly affected by the coefficient factor, but it was also related to the matching of the steel ratio and steel strength. These two methods only considered the comprehensive parameter of the confining effect, so there was a deviation between the calculation results. It should be pointed out that, due to the limitation of test data, the axial bearing capacity method of UHSCFST needs further research. Overall, the unified strength theory method is quite conservative for predicting the axial bearing capacity of UHSCFST. Therefore, (3) was used to calculate the axial bearing capacity of the UHSCFST with concrete strength grade up to C100 in Modaoxi Bridge.

5. Conclusions

Through the experiment of this paper, some conclusions can be drawn as follows:

(1) The UHSCFST short columns with core concrete strength grade up to C100 presented a drum-type failure mode under axial compression loads. The confining effect of the steel tube effectively avoided the brittle failure of C100 concrete and tremendously improved the axial load bearing capacity of the specimen.

(2) The UHSCFST short columns with a core concrete strength up to C100 have prominent ductility performance as the same of the ordinary CFST. The higher the confining effect, the better the ductility. And the plastic deformation ability of the specimen after load peak can also be increased obviously.

(3) The UHSC should be consisted of a high strength steel tube and a higher steel ratio, so as to obtain a formidable confining effect. Therefore, the load capacity of the postpeak would decline slowly or even remain unchanged. It is suggested that the C100 or above grade concrete should be combined with Q345 or above strength steel tube in UHSCFST, and the steel ratio should be no less than 20%.

(4) The influence of the confining effect should be taken into account when calculating the axial bearing capacity of UHSCFST short columns, and the axial bearing capacity can be calculated by the Chinese specification JTDG/T D65-60 in China.

Conflicts of Interest

The authors declare that they have no conflicts of interest.

Acknowledgments

The research is sponsored by Scientific Research Fund of Sichuan Provincial Education Department (15ZA0141, 16TD0018), the Transportation Science and Technology Project of Sichuan Province (2014C-7), and the Natural Science Foundation of Xihua University (z1420603). Their financial supports are gratefully acknowledged.

References

[1] T. Xie and T. Ozbakkaloglu, "Behavior of steel fiber-reinforced high-strength concrete-filled FRP tube columns under axial compression," *Engineering Structures*, vol. 90, pp. 158–171, 2015.

[2] T. Ozbakkaloglu, "Behavior of square and rectangular ultra high-strength concrete-filled FRP tubes under axial compression," *Composites Part B: Engineering*, vol. 54, no. 1, pp. 97–111, 2013.

[3] T. Ozbakkaloglu and B. L. Fanggi, "Axial compressive behavior of FRP-concrete-steel double-skin tubular columns made of normal- and high-strength concrete," *Journal of Composites for Construction*, vol. 18, no. 1, Article ID 04013027, 2013.

[4] D. Zhang, L. N. Huang, R. G. Wang, and J. H. Zhao, "Experimental study on mechanical properties of FRP tubular concrete columns," *Journal of Harbin University of C. E. & Architecture*, vol. 33, no. 1, pp. 73–76, 2000.

[5] S. Zhong, *he Unified Theory of CFST—Research and Application*, Tsinghua University Press, China, 2006.

[6] L. Han, *Concrete Filled Steel Tube Structure—Theory and Practice*, Science Press, China, 2007.

[7] S. Cai, *Modern Steel Tube Confined Concrete Structures*, China Communications Press, China, 2007.

[8] M. Xiong and J. Y. Richard Liew, "Design of high strength concrete filled steel tube columns for tall buildings," *Building Structure*, vol. 45, no. 11, pp. 37–42, 2015.

[9] K. Tan and X. Pu, "A study on the mechanical properties of steel tubular very high- strength concrete," *Journal of Southeast University*, vol. 29, no. 4, pp. 127–131, 1999.

[10] A. E. Kilpatrick and B. V. Rangan, "Tests on high-strength concrete-filled steel tubular columns," *ACI Structural Journal*, vol. 96, no. 2, pp. 268–274, 1999.

[11] E. Ellobody, B. Young, and D. Lam, "Behaviour of normal and high strength concrete-filled compact steel tube circular stub columns," *Journal of Constructional Steel Research*, vol. 62, no. 7, pp. 706–715, 2006.

[12] D. Liu and W.-M. Gho, "Axial load behaviour of high-strength rectangular concrete-filled steel tubular stub columns," *Thin-Walled Structures*, vol. 43, no. 8, pp. 1131–1142, 2005.

[13] J. M. Portolés, E. Serra, and M. L. Romero, "Influence of ultra-high strength infill in slender concrete-filled steel tubular columns," *Journal of Constructional Steel Research*, vol. 86, pp. 107–114, 2013.

[14] J. Y R Liew and D. X Xiong, "Experimental investigation on tubular columns infilled with ultra-high strength concrete," in *Tubular structures XIII*, pp. 637–645, Crc Press-Taylor & Francis Group, Boca Raton, Fla, USA, 2011.

[15] J. Y. Liew and D. X. Xiong, "Ultra-high strength concrete filled composite columns for multi-storey building construction," *Advances in Structural Engineering*, vol. 15, no. 9, pp. 1487–1504, 2012.

[16] Z. Tao, L.-H. Han, and D.-Y. Wang, "Strength and ductility of stiffened thin-walled hollow steel structural stub columns filled with concrete," *Thin-Walled Structures*, vol. 46, no. 10, pp. 1113–1128, 2008.

[17] S. Tokgoz and C. Dundar, "Experimental study on steel tubular columns in-filled with plain and steel fiber reinforced concrete," *Thin-Walled Structures*, vol. 48, no. 6, pp. 414–422, 2010.

[18] Y.-Y. Lu, N. Li, S. Li, and H.-J. Liang, "Experimental investigation of axially loaded steel fiber reinforced high strength concrete-filled steel tube columns," *Journal of Central South University*, vol. 22, no. 6, pp. 2287–2296, 2015.

[19] J. M. Portoles, M. L. Romero, J. L. Bonet, and F. C. Filippou, "Experimental study of high strength concrete-filled circular tubular columns under eccentric loading," *Journal of Constructional Steel Research*, vol. 67, no. 4, pp. 623–633, 2011.

[20] S. Zhang and Y. Wang, "Failure modes of short columns of high-strength concrete-filled steel tubes," *China Civil Engineering Journal*, vol. 7, no. 9, pp. 1–10, 2004.

[21] Y.-Y. Wang and S.-M. Zhang, "Experimental research on axially loaded high-strength concrete-filled steel tubes," *Journal of Harbin Institute of Technology*, vol. 36, no. 12, pp. 1646–1685, 2004.

[22] M.-X. Xiong and J. Y. R. Liew, "Mechanical behaviour of ultra-high strength concrete at elevated temperatures and fire resistance of ultra-high strength concrete filled steel tubes," *Materials and Design*, vol. 104, pp. 414–427, 2016.

[23] CECS 28-2012, "Technical specification for concrete-filled steel tubular structures," Tech. Rep., China Planning Press, Beijing, China, 2012.

[24] JTG/T D65-06—2015, "Specifications for Design of Highway Concrete -filled Steel Tubular Arch Bridges," Tech. Rep., China Communications Press, Beijing, China, 2015.

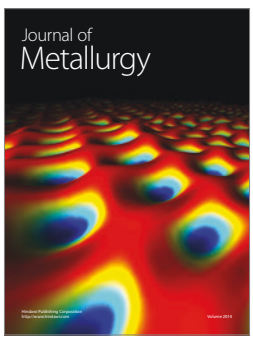

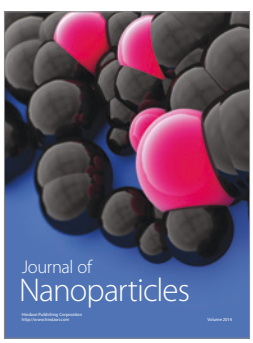

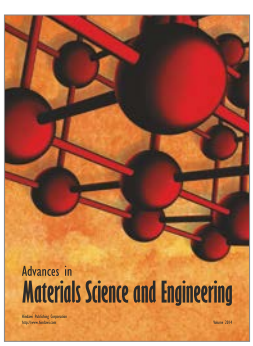

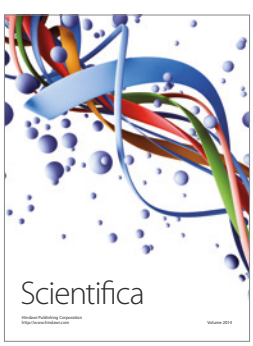

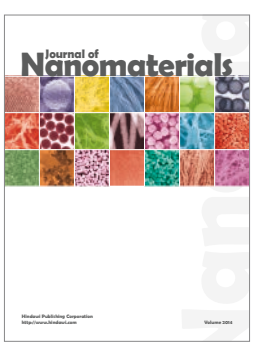

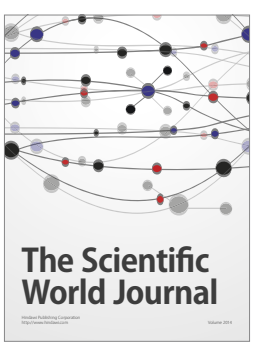

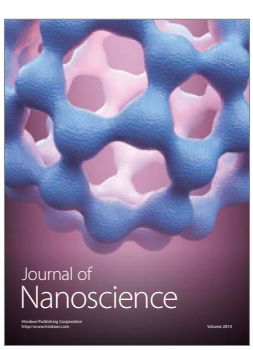

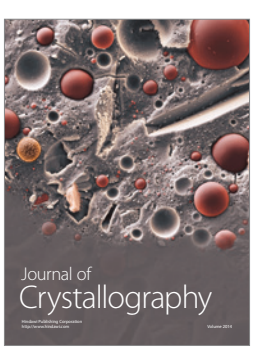

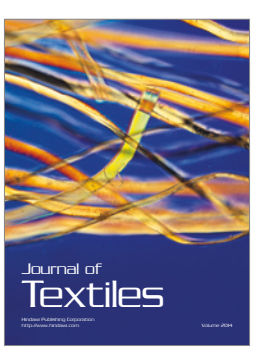

Hindawi

Submit your manuscripts at
https://www.hindawi.com